Probabilistic-deterministic transition involved in a fragmentation process of brittle materials: application to a high performance concrete

François Hild[a,*], Pascal Forquin[b], Christophe Denoual[c] and Xavier Brajer[d]

[a]LMT-Cachan, ENS de Cachan / CNRS-UMR 8535 / Université Paris 6
61 avenue du Président Wilson, F-94235 Cachan Cedex, France
[b]DGA/CTA-Département MSP, 16 bis avenue Prieur de la Côte d'Or
F-94114 Arcueil Cedex, France
[c]CEA/DAM-Département PTA, BP 12
F-91680 Bruyères le Chatel Cedex, France
[d]Saint-Gobain Recherche, 39 quai Lucien Lefranc
F-93303 Aubervilliers Cedex, France

Abstract

Dynamic loadings produce high stress waves leading to the fragmentation of brittle materials such as ceramics, concrete, glass and rocks. The main mechanism used to explain the change of the number of fragments with the stress rate is a shielding phenomenon. However, under quasi static loading conditions, a weakest link hypothesis may be applicable. Therefore, depending on the local strain or stress rate, different fragmentation regimes are observed. One regime corresponds to single fragmentation for which a probabilistic approach is needed. Conversely, the multiple fragmentation regime may be described by a deterministic approach. The transition between the two fragmentation regimes is discussed. A damage model describing dynamic fragmentation is applied to a high performance concrete.

Keywords: brittle materials, Continuum Damage Mechanics, discrete modeling, dynamic fracture, probability and statistics, single and multiple fragmentation, stress relaxation, Weibull model.

1 Introduction

A consequence of intense pulses on brittle materials is their fragmentation into discrete domains. For example, ceramics can be multiply fragmented when impacted [1]. Similarly, glass is used in armored windshields and experiences multiple fragmentation when impacted by debris or bullets [2–4]. Furthermore, since the pioneering work of Rinehart [5], it is known that the ultimate strength of rocks under so-called dynamic loading conditions exceeds the static strength by as much as one order of magnitude. The distinct zones resulting from rock blasting were

identified by Kutter and Fairhurst [6], namely a comminuted area in the vicinity of the explosive followed by a damaged zone in which dense microcracking is observed and finally a zone where few long cracks develop. Later, it was recognized that inherent flaws are activated, can grow and eventually coalesce to form macrocracks [7]. Similarly, concrete can experience multiple fragmentation when hit by a projectile [8]. Yet, when loaded in tension or flexure under quasi static conditions, the same materials usually experience single fragmentation and their failure strength is no longer deterministic. The aim of the present paper is to discuss the reasons for this difference in behavior and to propose criteria to account for both fragmentation regimes.

The fragmentation process is discrete by essence. In the theory developed by Mott [9], the fragmentation of a rapidly expanding ring was studied. It contains some key ingredients (*i.e.,* the randomness of the process is clearly stated and accounted for) to analyze the distribution of fragments in 2D experiments [10]. From a numerical point of view, discrete modelings are also proposed [11–14] when the fragment size is greater than or equal to the size of a representative element. Espinosa *et al.* [15] have developed a continuum/discrete multi-scale model in which the finer scale is discrete and allows for the derivation of a continuum description on a higher scale. Alternatively, Continuum Damage Mechanics can be used with an isotropic [16–18] or anisotropic [19] damage description to account for multiple fragmentation. Consequently, in the numerical simulations, the medium is assumed to be continuous on the scale of a finite element in which numerous cracks are expected to form. However, crack densities may strongly vary over the structure and the analysis of fragmentation through a continuum modeling may be delicate when one or a few cracks are nucleated or propagate in certain zones. As an alternative, a multi-scale model has been developed in which the probabilistic aspect is treated within a damage model [20, 21].

The aim of the present paper is to introduce relevant parameters that enable one to choose between continuum and discrete approaches. Section 2 introduces a fragmentation model accounting for quasi static and dynamic loading conditions. It is shown that a Poisson-Weibull framework is convenient to derive closed-form solutions. Characteristic parameters are introduced in Section 3. They depend on material properties (*i.e.,* Weibull parameters) and loading conditions (*i.e.,* strain or stress rate). A criterion is derived to discuss the transition between single and multiple fragmentation in terms of characteristic parameters. Based upon the fragmentation theory, a so-called multi-scale damage model [21] is summarized in Section 4. This model is used to analyze a so-called Edge-On Impact configuration [2] when used to study a high performance concrete in Section 5.

2   Fragmentation of brittle materials

For brittle materials, the analysis of failure depends upon the microstructure in terms of flaw density and failure stress distribution [7]. The microstructure is approximated by point defects of *density* λ_t. It can be described by a Poisson point process of intensity λ_t [22, 23]

$$\lambda_{\mathrm{t}}(\sigma) = \lambda_0 \left(\frac{\langle \sigma \rangle}{\sigma_0} \right)^m, \tag{1}$$

where m is the Weibull modulus, σ a local stress to be specified later on, σ_0 the scale parameter relative to a reference density λ_0, $\langle \star \rangle$ the Macauley brackets (*i.e.*, the positive part of $\star$). The constant λ_0/σ_0^m is the Weibull scale parameter. Equation (1) shows that the higher the local stress σ, the more defects can break. The probability P of finding $N = B$ cracks within a uniformly loaded domain Ω is expressed in terms of a Poisson distribution

$$P(N = B) = \frac{[\lambda_{\mathrm{t}}(\sigma)Z]^B}{B!} \exp\left[-\lambda_{\mathrm{t}}(\sigma)Z\right]. \tag{2}$$

The product $\lambda_{\mathrm{t}}(\sigma)Z$ corresponds to the average number of cracks within a domain Ω of volume, surface or length Z. Within the weakest link framework [24], the failure probability P_{F} is the probability of finding at least one crack in a domain Ω

$$P_{\mathrm{F}} = P(N \geq 1) = 1 - P(N = 0) = 1 - \exp\left[-Z\lambda_0 \left(\frac{\langle \sigma \rangle}{\sigma_0} \right)^m\right]. \tag{3}$$

When the domain is not uniformly loaded, the failure probability can be written as

$$P_{\mathrm{F}} = 1 - \exp\left[-Z_{\mathrm{eff}}\lambda_0 \left(\frac{\langle \sigma_{\mathrm{F}} \rangle}{\sigma_0} \right)^m\right], \tag{4}$$

where Z_{eff} denotes the effective volume, surface or length [25]

$$Z_{\mathrm{eff}} = \int_{\Omega} \left[\frac{\langle \sigma(\boldsymbol{x}) \rangle}{\sigma_{\mathrm{F}}} \right]^m \, \mathrm{d}\boldsymbol{x} \quad \text{with} \quad \sigma_{\mathrm{F}} = \max_{\Omega} \langle \sigma(\boldsymbol{x}) \rangle, \tag{5}$$

corresponding to an equivalent stress σ (*e.g.*, maximum principal stress) at a given point $\boldsymbol{x}$.

An ultra high performance concrete is analyzed in the sequel. This material (powder reaction concrete, commercial name: DUCTAL®) has a very fine microstructure made of components of different sizes, namely, fine quartz sand aggregates, cement, crushed quartz and silica fume [26]. For the sake of simplicity, the results reported herein only concern fiber-free grades for which a high compressive strength can be achieved but with a ductility comparable to conventional mortar. The ultimate strength of these materials can reach values of the order of -200 MPa to -800 MPa in uniaxial compression [27], and when reinforced by fibers the ductility is significantly increased. A residual porosity of the order of 2% is obtained in the present case and the compressive strength is equal to -200 MPa. Figure 1 shows a Weibull plot for 18 experiments on samples of size $11.2 \times 10.2 \times 150$ mm^3 submitted to three-point flexure (outer span: 130 mm). A Weibull modulus of 9.5 is obtained and $\sigma_0 = 23$ MPa when $1/\lambda_0 = 59$ mm^3 (i.e., identical to the effective volume).

Conversely, under impact, a whole cracking pattern is observed (see Section 5). It will be referred to as *multiple fragmentation* regime. In the following, it is assumed that the defect
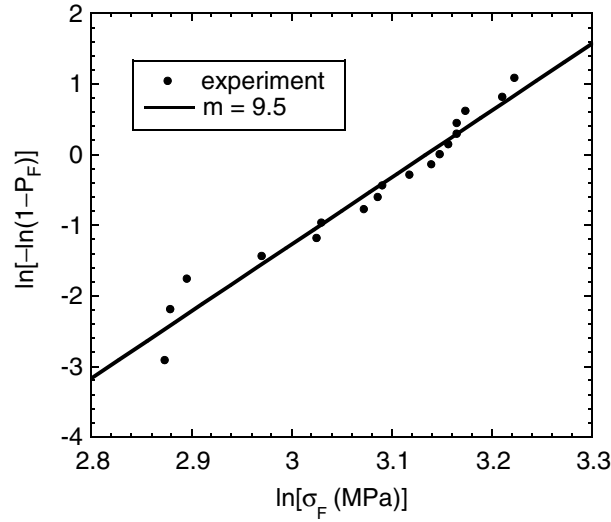
Figure 1: Weibull plot of Ductal® submitted to three-point flexure.

population leading to damage and failure is identical when the material is subjected to quasi static and dynamic loading conditions. To understand why a crack nucleates, one has to model the interaction of cracks and a defect that would initiate a crack. The crack propagation velocity is assumed to be constant and equal to a fraction k of the longitudinal wave speed C_0 [16,28,29]. Therefore, one may define a relaxation or obscuration domain of measure $Z_{\rm obs}$ around a crack (*i.e.,* a zone in which the stresses are less than the applied stresses, thus do not cause new crack initiations)

$$Z_{\rm obs} = S\left[kC_0\left(T - t\right)\right]^n, \tag{6}$$

which is a function of a shape parameter S, the present time T, the time to nucleation $t < T$, and the space dimension ($n = 1$, 2 or 3). The shape parameter S may depend on the Poisson's ratio ν but it is independent of time so that the relaxed zones are self-similar. New cracks will initiate only if the defect exists in the considered zone and if the flaw does not belong to *any* relaxed zone. Therefore, the total flaw density $\lambda_{\rm t}$ can be split into two parts: namely, $\lambda_{\rm b}$, the crack density and the obscured flaw density. The increment of the crack density $\lambda_{\rm b}$ can be related to that of total flaw density $\lambda_{\rm t}$ by

$$\frac{\mathrm{d}\lambda_{\rm b}}{\mathrm{d}t} = \frac{\mathrm{d}\lambda_{\rm t}}{\mathrm{d}t} \times \left(1 - P_{\rm obs}\right), \tag{7}$$

with $\lambda_{\rm b}(0) = \lambda_{\rm t}(0) = 0$ and $P_{\rm obs}$ the probability of obscuration [30]

$$P_{\mathrm{obs}} = 1 - \exp\left[-\widehat{Z}_{\mathrm{obs}}(T)\lambda_{\mathrm{t}}\left\{\sigma(T)\right\}\right], \tag{8}$$

where $\widehat{Z}_{\mathrm{obs}}$ is the measure of the mean obscuration zone

$$\widehat{Z}_{\mathrm{obs}}(T)\lambda_{\mathrm{t}}\left\{\sigma(T)\right\} = \int_0^T Z_{\mathrm{obs}}(T-t)\frac{\mathrm{d}\lambda_{\mathrm{t}}}{\mathrm{d}t}\left\{\sigma(t)\right\}\mathrm{d}t. \tag{9}$$

Equation (8) is an extension of the classical Weibull law (3). In particular, when the stress rate is small enough, only one defect leads to failure and $\widehat{Z}_{\mathrm{obs}} = Z$ and Eqn. (3) applies. It can be noted that Eqn. (8) accounts for overlappings of obscuration zones. Furthermore, in the context of mathematical morphology, the above-described approach is nothing but a boolean islands model [31, 32].

3 Characteristic parameters and fragmentation transition

Let us now consider a case with a constant stress rate $\mathrm{d}\sigma/\mathrm{d}t = \overset{\bullet}{\sigma}$. One can define a dimensionless flaw density ($\overline{\lambda} = \lambda/\lambda_{\mathrm{c}}$), time ($\overline{t} = t/t_{\mathrm{c}}$), zone size ($\overline{Z} = Z/Z_{\mathrm{c}}$) and stress ($\overline{\sigma} = \sigma/\sigma_{\mathrm{c}}$) from the condition

$$\lambda_{\mathrm{c}}\, Z_{\mathrm{c}} = 1 \ \ \mathrm{with} \ \ \lambda_{\mathrm{c}} = \lambda_{\mathrm{t}}[\sigma(t_{\mathrm{c}})] \ \ \mathrm{and} \ \ Z_{\mathrm{c}} = Z_{\mathrm{obs}}(t_{\mathrm{c}}), \tag{10}$$

where the subscript 'c' denotes characteristic quantities. A characteristic stress is defined by $\sigma_{\mathrm{c}} = \overset{\bullet}{\sigma}\, t_{\mathrm{c}}$. Equation (10) expresses the fact that the characteristic zone size Z_{c} contains *on average* one flaw that may break at the characteristic time t_{c}. By using Eqns. (1) and (10), the characteristic parameters are given by

$$t_{\mathrm{c}} = \left[\frac{\sigma_0^m}{\lambda_0 S(kC_0)^n\, \overset{\bullet}{\sigma}{}^m}\right]^{\frac{1}{m+n}}, Z_{\mathrm{c}} = \left[\frac{(\sigma_0 kC_0)^m S^{m/n}}{\lambda_0\, \overset{\bullet}{\sigma}{}^m}\right]^{\frac{n}{m+n}},$$

$$\sigma_{\mathrm{c}} = \left[\frac{\sigma_0^m\, \overset{\bullet}{\sigma}{}^n}{\lambda_0 S(kC_0)^n}\right]^{\frac{1}{m+n}}, \tag{11}$$

and a closed-form solution can be derived for Eqn. (7)

$$\overline{\lambda}_{\mathrm{b}}(\overline{T}) = \frac{m}{m+n}\left[\frac{(m+n)!}{n!m!}\right]^{\frac{m}{m+n}}\gamma\left[\frac{m}{m+n}, \frac{n!m!}{(m+n)!}\overline{T}^{m+n}\right], \tag{12}$$

where γ is the incomplete gamma function. Equation (12) is the *exact* solution to Mott's problem extended to 2D and 3D cases with an initial flaw density modeled by a power law function. Figure 2 shows the change of the dimensionless density $\overline{\lambda}_{\mathrm{b}}$ with the dimensionless

time $\overline{T}$. When the time $\overline{T} < 1$, virtually no obscuration is observed, *i.e.*, $P_{\mathrm{obs}} \approx 0$ and $\overline{\lambda}_{\mathrm{b}} \approx \overline{\lambda}_{\mathrm{t}}$. Conversely, when $\overline{T} \gg 1$, $P_{\mathrm{obs}} \approx 1$ and saturation occurs. The higher the Weibull modulus m, the higher the density at saturation.
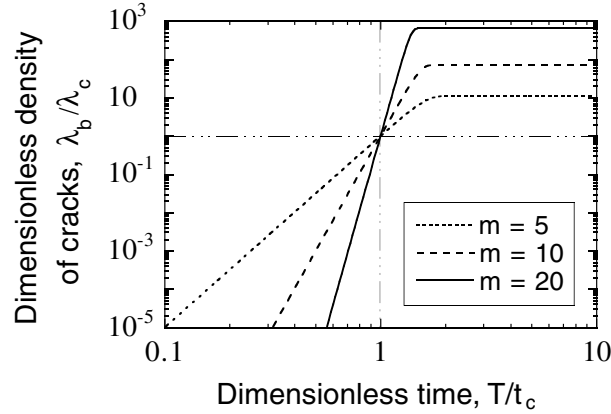

Figure 2:   Dimensionless density of cracks vs. dimensionless time for three different Weibull moduli m when $n = 3$.

A similar study is now carried out to determine the ultimate strength properties. Under quasi static loading condition, a Weibull model (3) is applied. It follows that the mean failure stress σ_{w} and the corresponding standard deviation σ_{sd} are given by

$$\sigma_{\mathrm{w}} = \frac{\sigma_0}{(Z_{\mathrm{eff}}\lambda_0)^{\frac{1}{m}}} \, \Gamma\left(1 + \frac{1}{m}\right) \, , \, \sigma_{\mathrm{sd}}^2 = \frac{\sigma_0^2}{(Z_{\mathrm{eff}}\lambda_0)^{\frac{2}{m}}} \, \Gamma\left(1 + \frac{2}{m}\right) - \sigma_{\mathrm{w}}^2 \qquad (13)$$

where *Gamma* is the Euler gamma function. It is expected that these quantities are the key parameters for low stress rates. In particular, no stress rate effect is obtained when sub-critical crack growth does not occur [33].

The variable P_{obs} can be used to define a damage variable in the framework of Continuum Damage Mechanics [30]. Under quasi static loading condition, there is a sudden change between the virgin material (*i.e.*, $D = 0$) and a fully broken brittle material (*i.e.*, $D = 1$). This case can be studied by using an *ad hoc* formulation [34, 35]. Under dynamic loading conditions, there is a more gradual growth. By averaging over a representative zone (to be specified later on), P_{obs} is *assumed* to be equal to the damage variable D. It is interesting to note that the first order approximation of Eqn. (8) leads to the differential equation proposed by Grady and Kipp [16] to describe the growth of an isotropic damage variable. By using Eqns. (1), (6) and (8), the change of the damage parameter is written as

$$D = 1 - \exp\left[-\frac{m!n!}{(m+n)!}\overline{\sigma}^{m+n}\right]. \qquad (14)$$

Equation (14) shows that $D(\overline{\sigma} = 1) \cong 0$ and $D(\overline{\sigma} = 2) \cong 1$ (*i.e.*, most of the damage evolution

occurs during a time interval equal to t_c). During t_c, the horizon is limited by $Z_{obs}(t_c) = Z_c$ therefore the *minimum* measure of the representative zone is Z_c. By noting that, in pure tension, the macroscopic stress Σ is related to the local (or effective) stress σ by $\sigma = \Sigma/(1-D)$ [37], the ultimate tensile strength $(\mathrm{d}\Sigma/\mathrm{d}\sigma = 0)$, denoted by Σ_{max}, is expressed as

$$\frac{\Sigma_{max}}{\sigma_c} = \left[\frac{1}{e} \frac{(m+n-1)!}{n!m!} \right]^{\frac{1}{m+n}}. \tag{15}$$

The normalized ultimate strength only depends upon the Weibull modulus m and the space dimension n. The ultimate strength itself is then proportional to $\overset{\bullet}{\sigma}{}^{n/(m+n)}$. This result is in agreement with experimental data of oil shale [16], microconcrete [36], ceramics and glass [4].

Equations (13) and (15) define two different regimes. The first one is obtained when a weakest link hypothesis is made. It corresponds to single fragmentation. The second one assumes multiple fragmentation. Figure 3 shows the change of the tensile strength with the stress rate for an effective volume V_{eff} $(n = 3)$ equal to $1/\lambda_0$. The lines represent analytical solutions while the dots and error bars are Monte-Carlo simulations (500 realizations per point). For a dimensionless stress rate less than 0.5, the ultimate strength is not modified by the loading rate and follows a classical Weibull model [see Eqn. (13)]. When it increases by approximately one order of magnitude, the ultimate strength follows the analytical solution (15). During the transition, the difference between the dashed lines [given by Eqns. (15) and (13)] and simulations does not exceed 10%. The standard deviation significantly decreases in the multiple fragmentation regime. Even if the ultimate strength has to be defined for static and dynamic loadings by a mean and a standard deviation, one can see that dynamic loadings lead to a more 'deterministic' behavior. The transition between 'quasi static' and 'dynamic' strength can be estimated by the intersection between the weakest link and the multiple fragmentation solutions (see Fig. 3)

$$\sigma_w = \Sigma_{max}(\overset{\bullet}{\sigma}). \tag{16}$$

The transition defined by Eqn. (16) leads to the following inequalities

$$\overset{\bullet}{\sigma} \begin{cases} < \overset{\bullet}{\sigma}_t & \text{single fragmentation} \\ \geq \overset{\bullet}{\sigma}_t & \text{multiple} \end{cases} \tag{17}$$

with

$$\overset{\bullet}{\sigma}_t = \sigma_0 k C_0 (\lambda_0 S)^{1/n} (Z_{eff} \lambda_0)^{(m+n)/mn} \left[\frac{e\, m!n!}{(m+n-1)!} \Gamma^{m+n} \left(\frac{m+1}{m} \right) \right]^{1/n}. \tag{18}$$

This transition does not only depend on material parameters but also involves the measure Z_{eff} of the considered element. The response of a large structure can be considered as 'dynamic' for low stress rates even if the material follows a weakest link hypothesis for the same loading applied on a smaller domain.
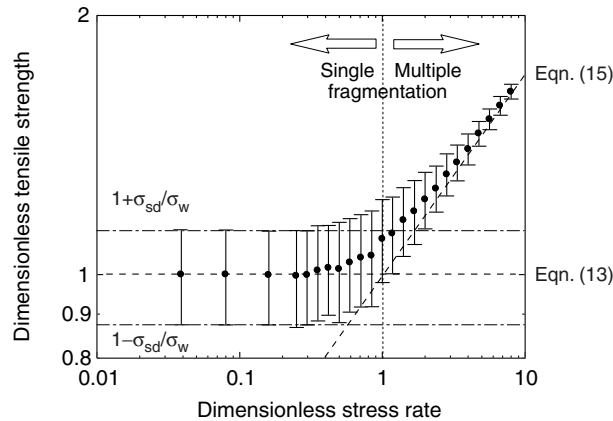
Figure 3: Tensile strength normalized by σ_w vs. stress rate normalized by $\dot{\sigma}_t$. The dots and error bars represent results obtained by Monte-Carlo simulations (500 realizations/point) and their standard deviation when $m = 9.5$ and $n = 3$. The curves are obtained by using Eqns. (13) and (15).

4 Multi-scale damage model

The state potential is assumed to be given by the Gibbs' specific enthalpy Φ. It is expressed as a function of the macroscopic stress tensor $\boldsymbol{\Sigma}$ and the damage variables D_1, D_2 and D_3 related to cracking in three orthogonal directions

$$\rho\Phi = \frac{1}{2}\,\boldsymbol{\Sigma} : \mathcal{S} : \boldsymbol{\Sigma} \tag{19}$$

where $\mathcal{S}$ is the compliance tensor dependent upon three damage variables D_1, D_2 and D_3 associated with three perpendicular cracking directions, ρ the mass density and ':' the contraction wrt. two indices. The associated forces are defined as

$$\boldsymbol{E} = \rho\frac{\partial\Phi}{\partial\boldsymbol{\Sigma}} = \mathcal{S} : \boldsymbol{\Sigma} \quad \text{and} \quad Y_i = \rho\frac{\partial\Phi}{\partial D_i} = \frac{1}{2}\,\boldsymbol{\Sigma} : \frac{\partial\mathcal{S}}{\partial D_i} : \boldsymbol{\Sigma} \tag{20}$$

where $\boldsymbol{E}$ denotes the strain tensor and Y_i the energy release rate density associated to the damage variable D_i $(i = 1, 2, 3)$. The compliance tensor $\mathcal{S}$ is expressed as (Voigt's notations are used)

$$
\mathcal{S} = \frac{1}{E}
\begin{bmatrix}
\frac{1}{1-D_1} & -\nu & -\nu & 0 & 0 & 0 \\
-\nu & \frac{1}{1-D_2} & -\nu & 0 & 0 & 0 \\
-\nu & -\nu & \frac{1}{1-D_3} & 0 & 0 & 0 \\
0 & 0 & 0 & \frac{1+\nu}{(1-D_2)^\alpha(1-D_3)^\alpha} & 0 & 0 \\
0 & 0 & 0 & 0 & \frac{1+\nu}{(1-D_3)^\alpha(1-D_1)^\alpha} & 0 \\
0 & 0 & 0 & 0 & 0 & \frac{1+\nu}{(1-D_1)^\alpha(1-D_2)^\alpha}
\end{bmatrix},
\quad (21)
$$

where the constant α is a function of the Poisson's ratio ν (when $\nu = 0.15, \alpha \approx 0.31$ [21]).

The growth of each damage variable D_i is based upon the defect density λ_t (no index summation is used)

$$
\frac{\mathrm{d}^2}{\mathrm{d}t^2}\left(\frac{1}{1-D_i}\frac{\mathrm{d}D_i}{\mathrm{d}t}\right) = n!S\left(kC_0\right)^n \widehat{\lambda}_t\left[\sigma_i(t)\right] \text{ when } \frac{\mathrm{d}\sigma_i}{\mathrm{d}t} > 0 \text{ and } \sigma_i > 0.
\quad (22)
$$

The cracking velocity kC_0 is about 20–40% the longitudinal wave velocity C_0 (*i.e.,* k is ranging between 0.2 and 0.4), and S is a dimensionless shape factor: in 3D situations $S \approx 3.74$ [21]. The effective stress tensor $\boldsymbol{\sigma}$ is related to the macroscopic stress tensor $\boldsymbol{\Sigma}$ by

$$
\mathcal{S}(D_1 = 0, D_2 = 0, D_3 = 0) : \boldsymbol{\sigma} = \mathcal{S}(D_1, D_2, D_3) : \boldsymbol{\Sigma}.
\quad (23)
$$

The stress σ therefore corresponds to any effective principal stress σ_i. The so-called multi-scale model uses a modified growth of the defect density (see also Ref. [20])

$$
Z_{\mathrm{FE}}\,\widehat{\lambda}_t[\sigma_i(t)] =
\begin{cases}
0 & \text{if } \sigma_i(t) \leq \sigma_{\mathrm{k}}, \\
\max\left[Z_{\mathrm{FE}}\,\lambda_0\left(\frac{\sigma_i(t)}{\sigma_0}\right)^m, 1\right] & \text{otherwise.}
\end{cases}
\quad (24)
$$

where σ_{k} is the failure stress of the first defect able to break. This failure stress σ_{k} is randomly generated according to a Weibull law (3) when $Z = Z_{\mathrm{FE}}$, where Z_{FE} is the volume of the considered finite element. The multi-scale model is therefore obtained by modeling the failure of the first defect able to break (which is scale-dependent, *i.e.,* mesh size dependent) in addition to the deterministic description of damage used in the continuous model. The probabilistic nature of crack nucleation then leads to numerical simulations that may vary between two different realizations.

An approximate closed-form solution can be derived. In Eqn. (24), one can assume that when the stress σ is less than σ_{k}, the density $\widehat{\lambda}_t$ is equal to 0. As soon as σ becomes equal to σ_{k}, the density $\widehat{\lambda}_t$ is equal to λ_t. Consequently, if t_{k} denotes the time when $\sigma = \sigma_{\mathrm{k}}$, the damage growth is given by

$$
D = 1 - \exp\left[-Z_{\mathrm{obs}}(T - t_{\mathrm{k}})\lambda_t\left\{\sigma(t_{\mathrm{k}})\right\} - \int_{t_{\mathrm{k}}}^{T} Z_{\mathrm{obs}}(T - t)\frac{\mathrm{d}\lambda_t}{\mathrm{d}t}\left\{\sigma(t)\right\}\mathrm{d}t\right].
\quad (25)
$$

When the applied stress rate is constant, Eqn. (24) can be recast as

$$D = 1 - \exp\left[-\left(\frac{t_{\mathrm{k}}}{t_{\mathrm{c}}}\right)^{m+n} \frac{m!n!}{(m+n)!} h(\tau, m, n)\right],$$ (26)

with

$$\tau = \frac{T}{t_{\mathrm{k}}} - 1 \quad \text{and}$$

$$h(\tau, m, n) = (1+\tau)^{m+n} - \left[1 + (m+n)\tau + \frac{(m+n)(m+n-1)}{2}\tau^2\right]$$ (27)

It can be noted that when $t_{\mathrm{c}}/t_{\mathrm{k}} \ll 1$, an ultimate strength equal to σ_{k} and the quasi static solution is obtained [Eqn. (13)]. Conversely, when $t_{\mathrm{c}}/t_{\mathrm{k}} \gg 1$, the dynamic regime is found with no scatter and Eqn. (14) applies so that the ultimate strength is deterministic [see Eqn. (15)].

The transition between the two regimes is re-analyzed. Figure 4 shows the change of the ultimate strength vs. stress rate for the same conditions as those of Fig. 3. The prediction of the average failure strength is obtained by assuming that the random stress σ_{k} is equal to σ_{w}. The corresponding standard deviation is evaluated by computing the failure strength corresponding to the value $\sigma_{\mathrm{k}} = \sigma_{\mathrm{w}} + \sigma_{\mathrm{sd}}$. These calculations lead to reasonable estimates. As expected, all results converge for low stress rates towards the closed-form solution given in Eqn. (13). Conversely, for high stress rates all solutions tend towards $\Sigma_{\max}$ expressed in Eqn. (15).
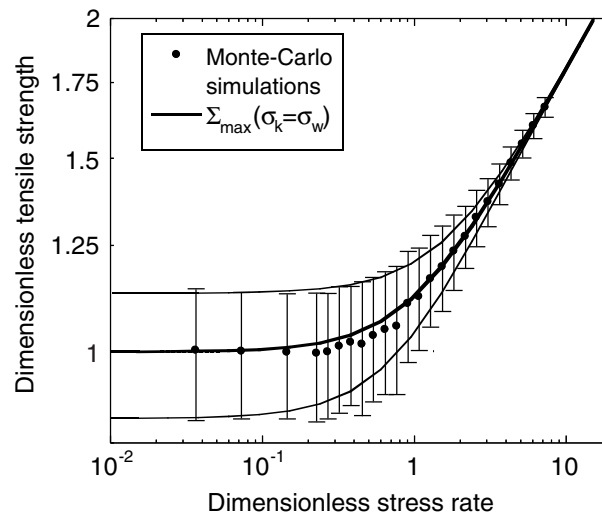

Figure 4:   Tensile strength normalized by σ_w vs. stress rate normalized by $\overset{\bullet}{\sigma}_t$. The dots and error bars represent results obtained by Monte-Carlo simulations (500 realizations/point) and their standard deviation when $m = 9.5$ and $n = 3$. The curves are obtained by using Eqn. (26).

5 Fragmentation of a high performance concrete

Tensile cracking, one of the major degradation mechanisms, can be observed during impact by using so-called Edge-On Impact (EOI) configurations instead of a real configuration where the degradation is 'hidden' in the bulk of the material. These configurations are developed by the Ernst-Mach-Institute (EMI) in Germany [1, 2] and by the Centre Technique d'Arcueil (CTA) in France [29, 38]. It can be shown that the same damage mechanism (i.e., damage in tension) is observed in EOI and in real impact configurations [39].

To avoid damage induced by the compressive wave close to the impact zone, a special setup is used (Fig. 5). It consists in creating an additional dynamic confinement obtained by using a steel ring containing a tungsten cylinder whose radius is greater than that of the projectile. This system creates an additional confinement during 12 μs (i.e., time duration for the wave to propagate back and forth in the steel ring) that prevents damage to develop in these zones by increasing the hydrostatic stress and reducing the deviatoric stress (i.e., less than 240 MPa for a distance greater than 12 mm from the impact point) to levels below the threshold of damage under confined conditions (i.e., of the order of 400 MPa [40]). When using a 2024 aluminum alloy projectile, this setup allows one to analyze fragmentation with no prior confined damage (i.e., hoop stresses greater than 35 MPa for a distance less than 80 mm from the impact point). Figure 6 shows a post-mortem observation when the tile is put in a sarcophagus to prevent the fragments to move too much. In this configuration, a blunt projectile (20 mm in diameter and 50 mm in length) impacts at 88 m/s a concrete plate of size $300 \times 150 \times 10$ mm^3. After impact, the tile is coated in an epoxy resin and polished for macroscopic (and microscopic) analyses.

Concrete plate
(300 x 150 x 10 mm^3)

Steel ring
(D_{ext} = 24 mm, h = 30 mm)

Tungsten alloy cylinder
(D = 13 mm, h = 30 mm)

Aluminum projectile
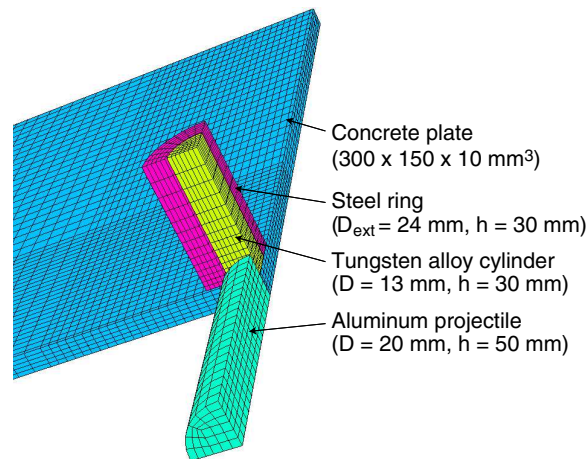(D = 20 mm, h = 50 mm)

Figure 5: One quarter of an edge-on impact configuration with dynamic confinement.

Once the elastic properties and the Weibull parameters are known, the model has no other parameters to tune apart from the crack propagation velocity. The velocity of a single crack

is estimated to be about 1875 m/s (i.e., the value of the parameter k is equal to 0.4). In the following, the predictive capability of the damage model to reproduce observed degradation patterns is evaluated. The simulation is performed for the confined EOI configuration with an impact velocity of 88 m/s. The random stress to failure is computed by using Eqn. (4) for a FE volume of 1 mm^3. Figure 7 shows the crack density associated to the first principal stress direction 35 μs after impact and at the end of the fragmentation process (*i.e.,* 50 μs). For high stress rates (*i.e.,* in front of the projectile and in the Hertz-like cone crack), many cracks nucleate in a FE cell. Failure of an element set, which can be compared to macroscopic cracks, can be observed in addition to the continuous degradation generated close to the impact zone. The *prediction* is in reasonable agreement with the experimental observations (Fig. 6), namely, a fine fragmentation in the first part of the plate followed by long radial cracks in the second half.
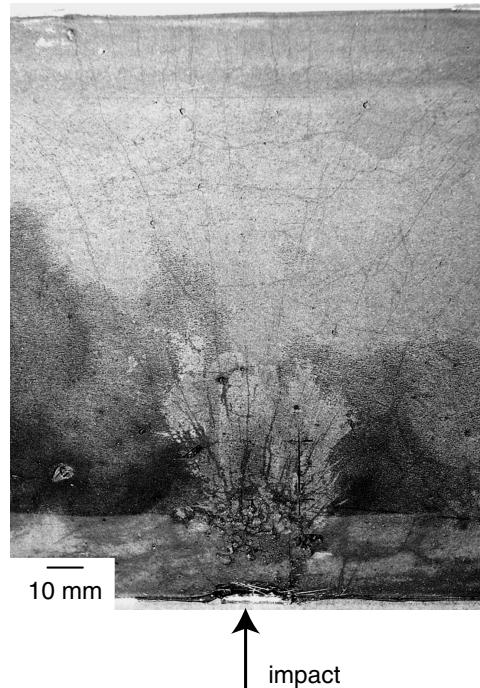

Figure 6:   Post-mortem view of an impacted Ductal® concrete plate by an aluminum projectile with a confined configuration.
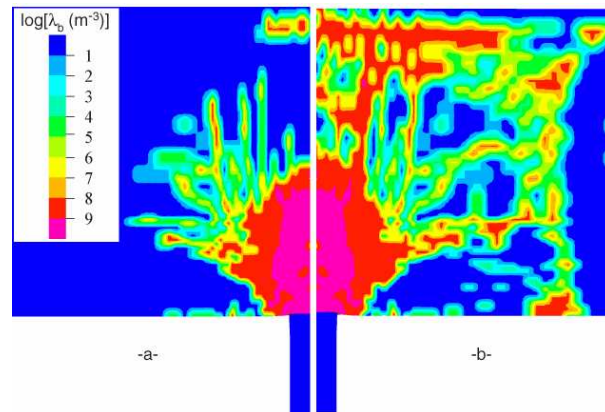
Figure 7: Contour of crack density associated to the first principal direction 35 μs (a) and 50 μs (b) after impact in a confined EOI experiment on Ductal®.

6 Summary

In this study, the defects in brittle materials are assumed to be randomly located in the zone of interest and their size distributions to follow a Poisson-Weibull model. A normalization procedure is defined by introducing characteristic quantities such as zone size, time and density of cracks. The dimensionless growth law for all the variables of the model is only dependent on the Weibull modulus and the space dimension. A damage growth and description is derived within a Continuum Damage Mechanics framework. The above-mentioned normalization technique is used to discuss the choice of the finite element mesh size. The characteristic size can be used as a measure of the representative zone, and defines the scale where the problem becomes deterministic and local.

The multi-scale model has been used to analyze cracking in Edge On Impact tests on an ultra-high performance concrete. A dynamic confinement was used to reduce or avoid confined damage close to the impact point. An intense fragmentation process made of numerous radial cracks is seen in post-mortem analyses. The damage model describing fragmentation enables us to get a good prediction of damage (pattern, cracking density and orientation) even if the density of cracking is slightly over-estimated. This can be explained by the low level of crack openings that are not easy to visualize.

References

[1] E. Strassburger, H. Senf, and H. Rothenhäusler. Fracture Propagation during Impact in Three Types of Ceramics, J. Physique IV coll. C8 [suppl. IV], pages 653–658, 1994.

[2] U. Hornemann, J. F. Kalthoff, H. Rothenhäusler, H. Senf, and S. Winkler. Experimental Investigation of Wave and Fracture Propagation in Glass - Slabs Loaded by Steel Cylinders at High Impact Velocities, EMI report E 4/84, Weil am Rhein (Germany), 1984.

[3] J. Cagnoux. Déformation et ruine d'un verre pyrex soumis à un choc intense: étude expérimentale et modélisation du comportement, Thèse d'Etat, University of Poitiers, 1985.

[4] F. Hild, X. Brajer, C. Denoual, and P. Forquin. On the Probabilistic-Deterministic Transition Involved in a Fragmentation Process of Brittle Materials, Comput. Struct. 81(12):1241–1253, 2003.

[5] J. S. Rinehart. Dynamic Fracture Strengths of Rocks, Proceedings 7th Symp. Rock Mech., (1965).

[6] H. K. Kutter and C. Fairhurst. On the Fracture Process in Blasting, Int. J. Rock Mech. Min. Sci., 8:181–202 1971.

[7] D. A. Shockey, D. R. Curran, L. Seaman, J. T. Rosenberg, and C. F. Petersen. Fragmentation of Rocks under Dynamic Loads, Int. J. Rock Mech. Min. Sci., 11:303–317, 1974.

[8] R. P. Kennedy. A Review of Procedures for the Analysis and Design of Concrete Structures to Resist Missile Impact Effects, Nucl. Eng. Des., 37:183–203, 1976.

[9] N. F. Mott. Fragmentation of Shell Cases, Proc. Roy. Soc. Lond, A189, 300–308, 1947.

[10] D. E. Grady and M. E. Kipp. Geometric Statistics and Dynamic Fragmentation, J. Appl. Phys., 58(3):1210–1222, 1985.

[11] N. Kusano, T. Aoyagi, J. Aizawa, Ueno, H. Morikawa, and N. Kobayashi. Impulsive Local Damage Analysis of Concrete Structure by the Distinct Finite Element Method, Nuclear Eng. Design 138:105–110, 1992.

[12] G. T. Camacho and M. Ortiz. Computational Modelling of Impact Damage in Brittle Materials, Int. J. Solids Struct., 33(20–22)¿2899–2938, 1996.

[13] S. Mastilovic and D. Krajcinovic. High-Velocity Expansion of a Cavity within a Brittle Material, J. Mech. Phys. Solids, 47:577–600, 1999.

[14] A. Ibrahimbegovic and A. Delaplace. Microscale and mesoscale discrete models for dynamic fracture of structures built of brittle material, Comput. Struct., 81(12):1255–1266, 2003.

[15] H. D. Espinosa, P. D. Zavattieri, and S. K. Dwivedi. A Finite Deformation Continuum/Discrete Model for the Description of Fragmentation and Damage in Brittle Materials, J. Mech. Phys. Solids, 46:1909–1942, 1998.

[16] D. E. Grady and M. E. Kipp. Continuum Modeling of Explosive Fracture in Oil Shale, Int. J. Rock Min. Sci. & Geomech. Abstr., 17:147–157, 1980.

[17] L. G. Margolin. Elasticity Moduli of a Cracked Body, Int. J. Fract., 22:65–79, 1983.

[18] A. M. Rajendran. Modeling the Impact Behavior of AD85 Ceramic under Multiaxial Loading, Int. J. Impact Eng., 15(6):749–768, 1994.

[19] C. Denoual and F. Hild. A Damage Model for the Dynamic Fragmentation of Brittle Solids, Comp. Meth. Appl. Mech. Eng., 183:247–258, 2000.

[20] W. Benz and E. Asphaug. Impact Simulations with Fracture. I. Method and Tests. Icarus, 107:98–116, 1994.

[21] C. Denoual and F. Hild. Dynamic Fragmentation of Brittle Solids: A Multi-Scale Model, Eur. J. Mech. A/Solids, 21:105–120, 2002.

[22] R. Gulino and S. L. Phoenix. Weibull Strength Statistics for Graphite Fibres Measured from the Break Progression in a Model Graphite/Glass/Epoxy Microcomposite, J. Mater. Sci., 26(11):3107–3118, 1991.

[23] D. Jeulin. Modèles morphologiques de structures aléatoires et changement d'échelle, thèse d'Etat, University of Caen, 1991.

[24] A. M. Freudenthal. Statistical Approach to Brittle Fracture, in: Fracture, H. Liebowitz, Edt., Academic Press, New York (USA), pages 591–619, 1968.

[25] D. G. S. Davies. The Statistical Approach to Engineering Design in Ceramics, Proc. Brit. Ceram. Soc., 22:429–452, 1973.

[26] P. Richard and M. Cheyrezy. Composition of reactive power concretes, Cement Conc. Res., 25(7):1501–1511, 1995.

[27] J. Dugat, N. Roux, and G. Bernier. Mechanical properties of reactive powder concretes, Mat. Struct., 29:233–240, 1996.

[28] L. B. Freund. Crack Propagation in an Elastic Solid Subjected to General Loading - Constant Rate of Extension, J. Mech. Phys. Solids, 20:129–140, 1972.

[29] P. Riou, C. Denoual, and C. E. Cottenot. Visualization of the Damage Evolution in Impacted Silicon Carbide Ceramics, Int. J. Impact Eng., 21(4):225–235, 1998.

[30] C. Denoual, G. Barbier, and F. Hild. A Probabilistic Approach for Fragmentation of Ceramics under Impact Loading, C. R. Acad. Sci. Paris, 325(Série IIb):685–691, 1997.

[31] D. Jeulin and P. Jeulin. Synthesis of Rough Surfaces by Random Morphological Functions, Proceedings 3rd European Symposium of Stereology, pages 239-246, 1981.

[32] J. Serra. Image Analysis and Mathematical Morphology, Academic Press, London (UK), 1982.

[33] A. G. Evans. A Method for Evaluating the Time-Dependent Failure Characteristics of Brittle Materials - and its Application to Polycrystalline Alumina, J. Mater. Sci., 7:1137–1146, 1972.

[34] H. D. Bui and A. Ehrlacher. Propagation dynamique d'une zone endommagée dans un solide élastique fragile en mode III et en régime permanent, C. R. Acad. Sci. Paris, série B(t. 290):273–276, 1980.

[35] H. D. Bui and A. Ehrlacher. Propagation of Damage in Elastic and Plastic Solids, in: Advances in Fracture Research, D. François, Edt., Pergamon Press, Oxford (UK), pages 533–551, 1982.

[36] A. Brara and J. Klepaczko. An Experimental Method for Dynamic Tensile Testing of Concrete by Spalling, Int. J. Impact Eng., 25:387–409, 2001.

[37] Y. N. Rabotnov. Creep Problems in Structural Members, North-Holland, Amsterdam (the Netherlands), 1969.

[38] C. Denoual, C. E. Cottenot, and F. Hild. Analysis of the Degradation Mechanisms in an Impacted Ceramic, in: S. C. Schmidt, D. P. Dandekar and J. W. Forbes, eds., Proceedings Shock Compression of Condensed Matter, AIP Press, New York (USA), pages 427–430, 1998.

[39] C. Denoual, C. E. Cottenot, and F. Hild. On the Identification of Damage during Impact of a Ceramic by a Hard Projectile, Proceedings 16th International Conference on BALLISTICS, APDS, Arlington, VA (USA), pages 541–550 ,1996.

[40] P. Forquin. Endommagement et fissuration de matériaux fragiles sous impact balistique, rôle de la microstructure, Ph.D. dissertation, Ecole Normale Supérieure de Cachan, 2003.